



Mechanical joining behavior of Cu–Fe dissimilar metallic foils in laser shock clinching

Chao Zheng¹ · Changdong Pan² · Jilai Wang³ · Guoqun Zhao¹ · Zhong Ji¹

Received: 3 February 2020 / Accepted: 10 August 2020 / Published online: 18 August 2020
© Springer-Verlag London Ltd., part of Springer Nature 2020

Abstract

Laser shock clinching is a novel joining method derived from laser shock forming in which the metal foil is plastically deformed under the pulsed laser induced shock wave, and then two or more metal foils can be joined together based on plastic deformation. However, the present researches are less concerned with the mechanical joining behavior of metal foils during incremental impacts of multiple laser pulses. In the present study, the mechanical joining behavior of pure copper foil and pre-pierced stainless steel sheet in laser shock clinching was investigated. A finite element model was established to analyze the material flowing and clinching behavior of metal foils under multiple laser pulses. Based on the validated model, the deformation stages, thickness change, and shock wave propagation features were studied. The temperature rise during clinching was assessed considering both the compression by shock wave and plastic deformation at high strain rates. It is revealed that the laser shock clinching process can be divided into three deformation stages, that is, free bulging forming, radial expansion, and formation of interlock. Both experimental and numerical results prove that the formation of clinched joints relies on the plastic deformation of the joining partner I. The thinnest region of the joint locates at the material of the joining partner I in contact with the upper corner of the joining partner II. In addition, there is no obvious influence of temperature increase on the mechanical properties of joining partners. Moreover, the shock wave propagation characteristics along axial direction and the influence of laser power density on interlock value and thickness distribution were also discussed.

Keywords Laser shock clinching · Laser shock forming · Mechanical joining · Numerical simulation · Plastic deformation

1 Introduction

The effective joining of dissimilar materials, such as various metallic materials or metallic and nonmetallic materials, provides the possibility to form multi-material hybrid structure widely demanded in a broad range of industries. This specific connection can optimize the design of component materials of products, and weight reduction can be realized as well as the

improvement of service performance [1]. Thus, the joining of dissimilar materials is a key concern in many fields across the macro, meso, and micro levels.

Laser welding is regarded as one of effective and efficient joining techniques, especially in the field of micro-joining. Due to the high power density provided by the focused laser beam, the local area of dissimilar materials is heated and cooled rapidly, resulting in a quite small heat affective zone. It is beneficial for the joining of thin metal sheets generally required in mechanical, electronic, and energy components. Compared with other joining methods, laser welding holds advantages of non-contact, flexibility, and high precision, and is suitable for most materials [2]. Shi et al. [3] carried out experiments on micro-laser welding of copper wire to aluminum pin of electronic components. The copper wire is melted due to the irradiation of pulsed laser and then the molten copper coats the aluminum pin, leading to the fusion of aluminum and formation of Cu–Al compound. Zimmer et al. [4] proposed laser micro-riveting technique for the joining of dissimilar thin films. It is found that a hollow rivet of copper is achieved under the pulsed laser

✉ Chao Zheng
zhengchao@sdu.edu.cn

¹ Key Laboratory for Liquid–Solid Structural Evolution and Processing of Materials (Ministry of Education), School of Materials Science and Engineering, Shandong University, 17923 Jingshi Road, Jinan 250061, People’s Republic of China

² Hyundai Motor R&D Center, 500 Changjiang Road, Yantai 264000, People’s Republic of China

³ School of Mechanical Engineering, Shandong University, 17923 Jingshi Road, Jinan 250061, People’s Republic of China

irradiation, which connects the copper film with the overlaying molybdenum film by geometrical interlock. Lerra et al. [5] evaluated the influence of laser pulse shape and separation distance on the metallurgical, mechanical, electrical, and thermal properties of Al–Cu lap joints in pulsed laser welding. The experimental results show that the pulse shape with an increasing step can obtain high maximum tensile load compared with that with a decreasing step. Nevertheless, the difference in material properties brings about the low weldability between dissimilar thin metal sheets, resulting in many challenges using laser welding technique. According to the investigation conducted by Shi et al. [6], the formation of weld defects such as hot cracks and blowholes in the Cu–Al joint by micro-laser welding cannot easily be mitigated due to the differences of physical properties and lattice constants between copper and aluminum. Chen et al. [7] analyzed the weld cracks that appeared in micro-laser welding of NiTiNb shape memory alloy and Ti6Al4V alloy. Their observations identify that different kinds of cracks can be found in the joints, which is mainly attributed to the formation of brittle intermetallic compounds. As a consequence, much more concerns are needed to suppress the weld defects and improve the service performance of joints for laser welding of dissimilar materials.

It is well known that as the laser power density enhances, the interaction between laser and material becomes stronger. While the laser power density of a beam is up to GW/cm^2 level, a plasma will be formed followed by a shock wave with high amplitude pressure, resulting in the deformation or fracture of the incident target [8]. Based on the aforementioned physical principle, laser shock welding has been proposed which is a solid-state impact welding technique similar to explosive welding and magnetic pulse welding. In laser shock welding process, a flyer and a target are metallurgically joined by a plasma-based pressure at high strain rates, and no liquid pool appears which generally exists in laser welding [9]. It has been detected that the flyer velocity can reach up to 1000 m/s within $0.2 \mu\text{s}$ [10]. Therefore, laser shock welding provides an approach to join both similar and dissimilar materials. Wang et al. [11] evaluated the feasibility of joining aluminum/aluminum and aluminum/copper thin sheets through laser shock welding. The examination on the interface of joints shows that the interface of dissimilar metals is flatter than that of similar materials. In order to better control the laser shock welding process, a suitable laser system with diagnostics is established, and a CNC-based three-axis welding apparatus is built from the perspective of high production efficiency [12]. Besides the effective connection of thin metal sheets, a fine wire can be welded to a metal sheet by laser shock welding, exhibiting its advantages for broad industry application [13]. However, the laser beam with very high energy is needed to accelerate the flyer to impact the target and destroy the oxidation film on the metal surface. In this case, spallation may occur due to the generated ultrahigh shock wave pressure, resulting in the strength degradation of welded joint [14].

It is noted that the materials couples are welded based on metallurgical joining for both laser welding and laser shock welding techniques. Since there are big gaps between dissimilar materials in terms of melting point, thermal conductivity, and electrical resistivity, in some cases it is quite difficult to realize the high-quality connection through welding approach [15]. In recent years, joining processes based on plastic deformation of one or two joining partners have attracted much more attention, such as clinching, riveting, hemming, and hydroforming [16]. Each process holds its specific technological superiority in the joining field, especially in the joining of dissimilar materials. In comparison with the welded joints originated from the metallurgical joining of partners, the mechanical joints are formed according to the plastic joining principle and then the form- and force-closed joints can be achieved.

Laser shock clinching, a novel joining method derived from laser shock forming, is firstly proposed by Ji et al. [17]. In this process, the metal foil is plastically deformed under the pulsed laser induced shock wave, and then two or three metal foils can be joined together based on plastic deformation. Laser shock clinching possesses the characteristics of laser shock processing, clinching, and high-velocity joining, and thus is suitable for the joining of dissimilar materials, especially in micro range [18]. Veenaas et al. [19] experimentally investigated the clinching of aluminum foil to the pre-pierced stainless steel foil by laser shock. Based on the observation of the cross-section of joints, it is explored that the formation of the joint is because of the mechanical interlock of the upper aluminum foil to the lower steel foil. Further experiments found that the first 10 laser pulses can introduce relatively large plastic strains compared with those under subsequent pulses [20]. Wang et al. [21] proposed a micro-clinching process compounded with cutting by laser shock forming in which a creative joining device was designed. Under the effect of laser-induced shock wave, the lower metal foil is firstly cut off and then the upper one plastically deforms to form an interlock with the remaining lower foil. The influence of absorbent coating, soft punch, die depth, and pulsed laser energy on neck thickness and interlock value was discussed by a series of experiments [22]. It is found that the reasonable organization of basic processing parameters is critical to make the dissimilar materials joinable. Ji et al. [23] established a finite element model to analyze the effect of laser energy and die depth on the formation of interlock between pure copper foil and pre-pierced stainless steel sheet. The results show that the moderate laser energy and die depth are crucial in the acquirement of high-quality joints. Moreover, the attempt to join three partners by laser shock clinching was conducted using two pure copper foils and a pre-pierced stainless steel sheet [24]. Recently, the shear clinching [25] and line clinching [26] by laser shock have been achieved to expand the application range of laser shock clinching technique.

Due to the ultrashort interaction time between laser and material, the plastic deformation of metal foils and the

formation of interlock structure are accomplished within several microseconds. Thus, it is difficult to entirely capture the material flowing and deformation characteristics of dissimilar materials in laser shock clinching by using experimental detection. On the other side, the present numerical simulation researches are less concerned with the mechanical joining behavior of metal foils during incremental impacts of multiple laser pulses. In addition, the temperature increase and shock wave propagation in laser shock clinching have not been well understood, which may affect the clinching process of metal foils. In this sense, it is full of the importance to reveal the mechanical joining behavior of dissimilar metal foils in laser shock clinching through a detailed investigation.

In the present study, the mechanical joining behavior of pure copper foil and pre-pierced stainless steel sheet in laser shock clinching was investigated. A finite element model was established to analyze the material flowing and clinching behavior of metal foils under multiple laser pulses. Based on the validated model, the deformation stages, thickness change, and shock wave propagation features were studied. The temperature rise during clinching was assessed considering both the compression by shock wave and plastic deformation at high strain rates. Moreover, the influence of laser power density on interlock value, thickness distribution, and the maximum thinning rate was also evaluated.

2 Experiments

2.1 Mechanism of laser shock clinching with pre-pierced hole

Figure 1 presents the schematic diagram of laser shock clinching process. A Nd:YAG laser is employed to produce a beam with the laser power density higher than 10^{12} W/m². While the high-energy laser beam irradiates the target, a

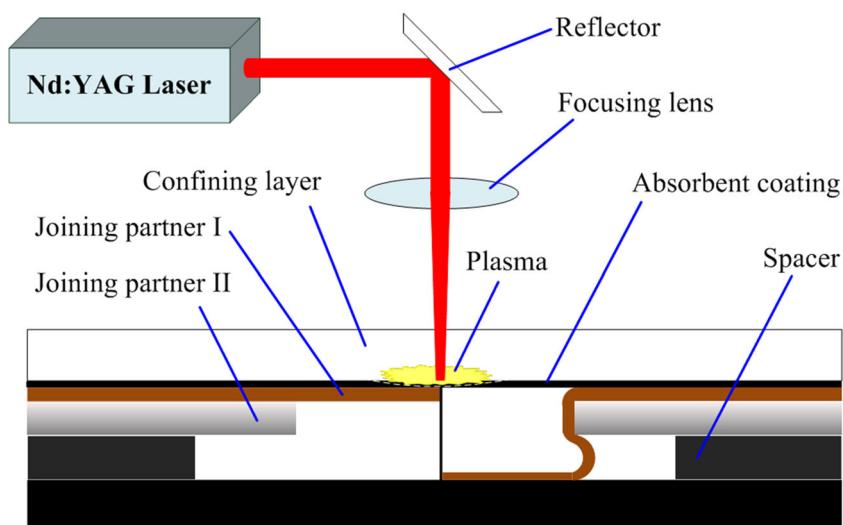
plasma will be generated with high pressure and temperature. Then the rapid expansion of the plasma induces a shock wave, which subsequently propagates into the target and further causes plastic deformation if the amplitude of shock wave pressure is beyond the dynamic yield strength of the target. In order to prevent the target from laser ablation, an absorbent coating is generally adopted, such as black paint, ink, graphite, and aluminum foil, to interact with the incident laser beam instead of the target. For the sake of amplification of shock wave pressure, a confining layer is usually used to restrain the free expansion of the plasma. Water or glass is often chosen to act as the confining layer.

The laser shock clinching process concerned in this study is one of joining partners pre-pierced before clinching. In such circumstance, two materials with significant difference in plasticity and strength are able to clinch together. The piercing process is generally applied to the joining material with lower plasticity or higher strength. As seen in Fig. 1, the pre-pierced joining partner II locates beneath the joining partner I. Under the incremental effect of laser pulses, the joining partner I is deformed plastically and flows into the cavity composed of joining partner II, spacer, and base. The joint is finally formed until the appropriate interlock value has been achieved.

2.2 Experimental setup

The experiments were implemented by a Nd:YAG laser with the wavelength of 1064 nm and the pulse duration of 7.3 ns. The laser beam with Gaussian spatial distribution is transmitted by a reflector and then converged using a focusing lens. Quartz glass with the thickness of 3 mm was employed to serve as the confining layer, and ink was used as the absorbent coating of about 80 μm in thickness, which was pre-coated on the glass surface facing metal foil. The choice of ink is because of its high efficiency of laser energy absorption and easy removal after the clinching process. The spot diameter on the

Fig. 1 Schematic diagram of laser shock clinching process



ink surface was about 2 mm to ensure that the laser power density is high enough to cause plastic deformation. The pulse frequency was 1 Hz and the spacer height was 150 μm . It is noted that part of the ink will be consumed owing to laser ablation while each laser pulse has been imposed. Thus, after five laser pulses are applied, the position of the quartz glass will be adjusted to guarantee the protection of ink.

2.3 Specimen preparation

T2 pure copper foil with the thickness of 30 μm was chosen as the joining partner I. The as-received pure copper foil was annealed in a vacuum furnace at the temperature of 450 $^{\circ}\text{C}$ for 1 h to eliminate the rolling direction effect, and then an average grain size of 12 μm in the thickness direction was gained. 304 stainless steel with the thickness of 100 μm was used to act as the joining partner II. Before laser shock clinching process, a hole with a specific diameter needs to be fabricated on the stainless steel sheet. Figure 2 compares the wall morphology of pierced holes by drilling and laser drilling, respectively. It can be seen that the burr distinctly appears on the hole wall obtained by drilling, which may hinder the metal flowing of the joining partner I and further result in the premature fracture, shown in Fig. 2a. However, the hole wall exhibits good forming quality while laser drilling with a fiber laser cutting machine is performed, as seen in Fig. 2b. The diameter of the pre-pierced hole is 2 mm in the experiments.

After laser shock clinching process, the joint was cut apart along the meridian plane, and then both the cross-section morphology and the interlock value were examined using a DX-200 digital microscope.

3 Numerical modeling

3.1 Analysis scheme

The ABAQUS software was adopted to implement the numerical simulation of laser shock clinching and to attempt to explore the mechanical clinching behavior of the material in the process.

Fig. 2 Wall morphology of pre-pierced hole by drilling (a) and laser drilling (b)

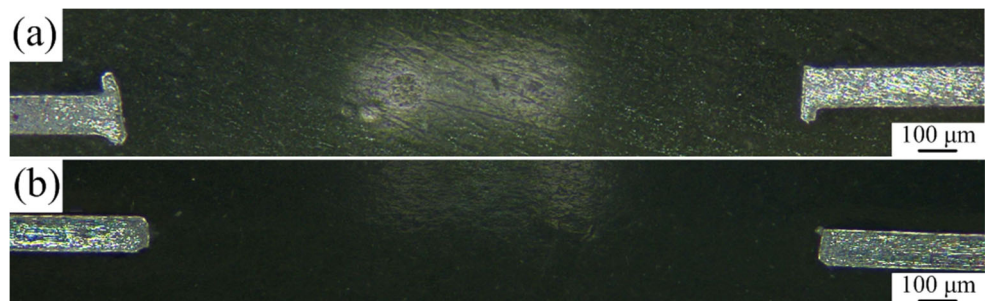


Figure 3 shows the finite element analysis scheme of laser shock clinching. The finite element model was established considering the necessary pre-treatment, such as materials properties description, shock wave loading, boundary condition setting, and so on. Due to the ultrashort acting time of shock wave pressure, the materials are deformed at relatively high velocity. Thus, ABAQUS/Explicit module was adopted to analyze this transient plastic deformation under a series of laser pulses. After all of the preset pulses have been applied, the springback analysis was then conducted through ABAQUS/Standard module to obtain a stable deformation status.

3.2 Finite element modeling

In the confining regime, the shock wave pressure induced by a high-energy pulsed laser can be assessed by the equation [27]

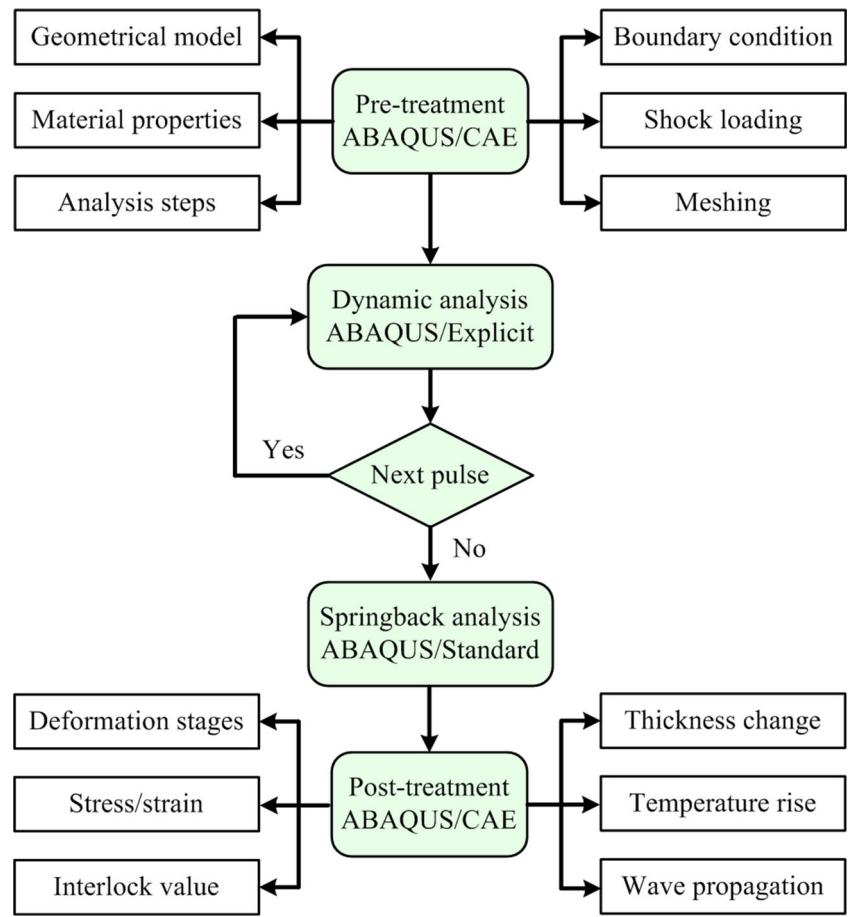
$$P_{\max} = 10^{-9} \sqrt{\left(\frac{a}{2a+3}\right)} \cdot Z \cdot I_0 \quad (1)$$

where P_{\max} is the peak value of shock wave pressure and a is the energy conversion coefficient usually regarded as 0.1; I_0 is the applied laser power density per pulse; and Z is the shock impedance related to the interaction between the metal foil Z_1 and the confining overlay Z_2 , expressed as $2/Z = 1/Z_1 + 1/Z_2$. In the current research, the shock impedance of quartz glass and pure copper is 1.31×10^7 and 4.18×10^7 $\text{kg/m}^2\text{s}$, respectively [28].

The temporal evolution of laser-induced shock wave pressure can be simplified to a triangular shape, as shown in Fig. 4a. The spatial distribution of the pressure is generally considered to obey Gaussian spatial distribution similar to that of laser beam. Thus, the shock wave pressure at the moment t and the position r can be written as $P_{(r,t)} = P_{(t)} \exp(-r^2/2r_0^2)$, in which r is the distance from the center of laser spot and r_0 is the radius of spot. Figure 4b presents the calculated spatial distribution shape of the pressure. The subroutine VDLOAD was used to accomplish the multiple loading of laser pulses.

Johnson–Cook constitutive model was adopted to describe the stress–strain relationship of pure copper and stainless steel. This model is generally used in laser shock processing, given by [29]

Fig. 3 Finite element analysis strategy of laser shock clenching



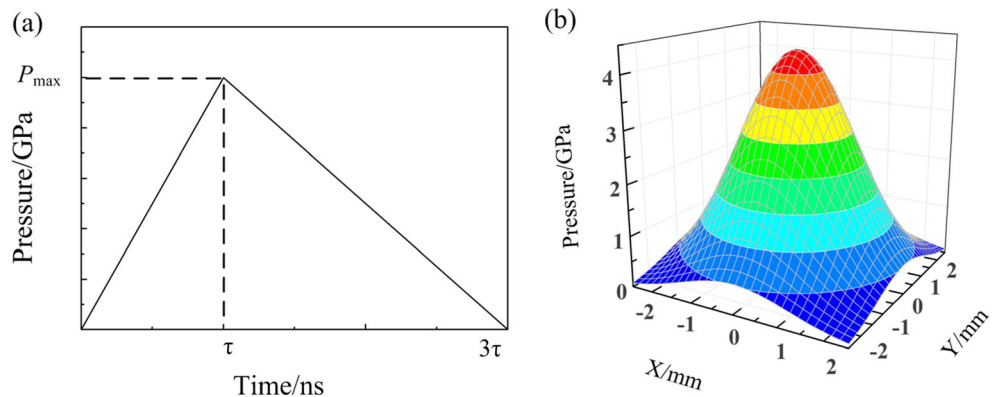
$$\sigma = (A + B\varepsilon^n) \left(1 + C \ln \frac{\dot{\varepsilon}}{\varepsilon_0} \right) \left[1 - \left(\frac{T - T_r}{T_m - T_r} \right)^m \right] \quad (2)$$

where σ is the dynamic yield strength of the material; ε is the plastic strain; $\dot{\varepsilon}$ is the strain rate; ε_0 is the reference strain rate (generally 1/s); and T , T_r , and T_m is the environment temperature during the process, room temperature, and the melting point of the material, respectively. Since the absorbent coating prevents the metal foil from being ablated by pulsed laser beam, the temperature softening effect can be ignored. For

pure copper, $A = 90$ MPa, $B = 292$ MPa, $C = 0.025$, and $n = 0.31$; for stainless steel, $A = 350$ MPa, $B = 275$ MPa, $C = 0.022$, and $n = 0.36$ [29].

Figure 5 presents the established finite element model of laser shock clenching. Due to the fact that the shapes of both laser spot and clinched joint are circular, an axisymmetric simplification was adopted. The joining partner I is pure copper foil with the thickness of 30 μm , while 304 stainless steel of 100 μm in thickness is chosen as the joining partner II. The diameters of both laser beam and pre-pierced hole on the joining partner II are 2 mm. The height of the spacer is 150 μm ,

Fig. 4 Characteristics of shock wave pressure. **a** Temporal evolution; **b** spatial distribution



and a flat bottom plate is used to limit the deformation along z -axis. The blank holder force was set to 5 kN to compress the materials below the blank holder. Element CAX4R was adopted to mesh the joining partners. In order to fully capture the high-strain-rate plastic deformation during laser shock clinching, part of the region slightly larger than the diameter of laser beam on the joining partner I has been refined using smaller element sizes.

3.3 Determination of explicit analysis time

The determination of explicit analysis time is one of noteworthy concerns while the finite element calculation is implemented. Obviously, the dynamic deformation characteristics of the joining partners cannot be fully captured while the analysis time is not enough. On the other side, there is a waste of time if the analysis time is set too long. Thus, the reasonable explicit analysis time for each laser pulse in the simulation needs to be ascertained.

In the present model, the laser power density is 6.76×10^{12} W/m², and the explicit analysis time for a single laser pulse was initially set to 35 μ s. The balance of internal energy for the whole numerical simulation model and the variation of each energy component were adopted to evaluate the explicit analysis time. The internal energy E_I can be expressed as

$$E_I = E_A + E_P + E_E \quad (3)$$

where E_A is the artificial strain energy, E_P is the energy dissipated by plasticity, and E_E is the applied elastic strain energy.

Figure 6 shows the evolution of the internal energy components under a single laser pulse. It can be seen that the values of E_I and E_P are almost the same while E_A and E_E are nearly equal to zero, suggesting that almost all of the internal energy have converted into the energy consumed by the

plastic deformation of materials. Furthermore, it is noted that after 3 μ s, there are no significant changes for E_P and its value keeps constant within the following time, indicating that no further plastic deformation takes place. Considering the fact that multiple laser pulses are imposed during the process and the collision between the material and the bottom plate may have an effect on the plastic deformation behavior, the calculation time in explicit dynamic analysis for each laser pulse is finally set to 6 μ s in the simulation.

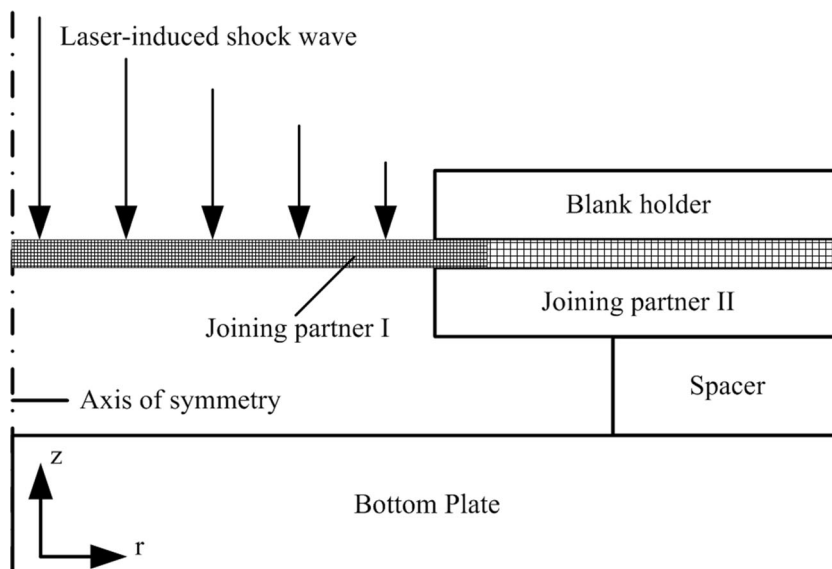
4 Results and discussion

4.1 Simulation model validation

After laser shock clinching process, the residual ink spread on the joint surface was removed using an ultrasonic cleaner, and then anhydrous alcohol was adopted to clean the joint surface. The general view of the joint is shown in Fig. 7a, in which 25 pulses with the laser power density of 6.76×10^{12} W/m² have been applied. In order to examine the surface quality of the clinched joint, amplification of the center of the surface facing laser beam was carried out by scanning electron microscope, as shown in Fig. 7b. It is manifest that there is no obvious evidence of laser ablation on the joint surface, suggesting that the formation of the joint is mechanical through the effect of laser-induced shock wave. This is attributed to the protection from the absorbent coating and the application of relatively low laser power density.

In order to better analyze the mechanical joining behavior of the materials during laser shock clinching, some zones within the joining partner I are specially concerned, as illustrated in Fig. 8. Zone A and zone B are related to the material of the joining partner I in contact with the upper and lower

Fig. 5 Finite element model of laser shock clinching



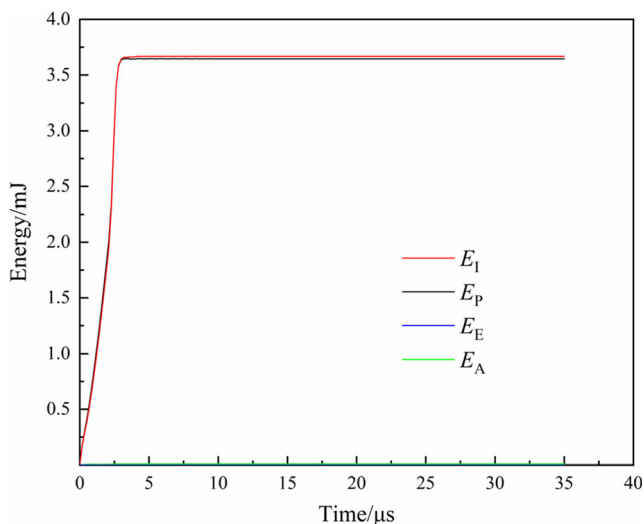


Fig. 6 Evolution of the internal energy components

corner of the joining partner II, respectively. Zone C correlates to the material on the boundary touching the bottom plate. In addition, t_u is defined as the interlock value to represent the clinching degree of the joints.

Figure 9 presents the comparison of numerical simulation and experimental measurements in terms of t_u with various laser pulses. It can be seen that across the whole process, the numerical results exhibit a good agreement with those of experiments, suggesting that the established finite element model is reliable and can be employed to carry out further investigations. Moreover, it is noted that the joining partner II keeps its original state even after 25 laser pulses in both numerical simulation and experiments. It implies that no obvious plastic deformation occurs for the stainless steel under the given processing parameters due to its high strength in comparison with that of pure copper foil. Therefore, the formation of clinched joints relies on the plastic deformation of the joining partner I, which will be paid special attention in the following sections.

It is noticeable that there are some differences between the numerical simulation and experimental measurements, as shown in Fig. 9. It may be attributed to (1) the deviation of the calculated shock wave pressure compared with the actual value and (2) the difference in the mechanical property of pure copper foil between the fitting constitutive model and reality.

The development of interlock value is closely associated with the formation of the clinched joint, and obviously the interlock value has important ties with the applied pulsed laser parameters, such as laser power density and number of pulses. Thus, it is of great significance in analyzing the evolution of the interlock value during the process. Figure 10 presents the changes of interlock values with the number of laser pulses through both numerical and experimental approaches. Five specimens have been checked in the experiments, and both the average and deviation have been given in Fig. 10.

It can be seen that while the number of laser pulses is less than 15, there is no significant indication on the formation of interlock. After 15 pulses have been applied, the interlock starts forming and its value increases with the action of more pulses. Both the numerical simulation and experimental results present the same trend, which gives a further verification of the established finite element analysis model. Furthermore, it is clearly seen that while 25 pulses have been applied, a joint with a moderate interlock value has been obtained. The deviation between the predicted and practical interlock values is less than 10%.

4.2 Deformation stages

According to the plastic deformation behavior of the joining partner I, the laser shock clinching process can be divided into three deformation stages, as shown in Fig. 11. The first stage relates to the free bulging forming, while radial expansion occurs in the second stage. As the joining partner I entirely

Fig. 7 Morphology of the clinched joint. **a** General view of the joint; **b** amplification of the center of the surface

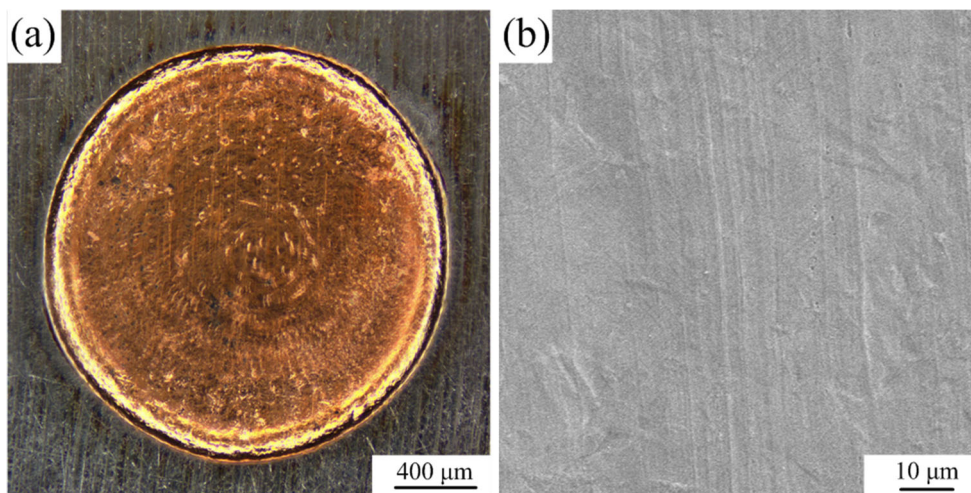
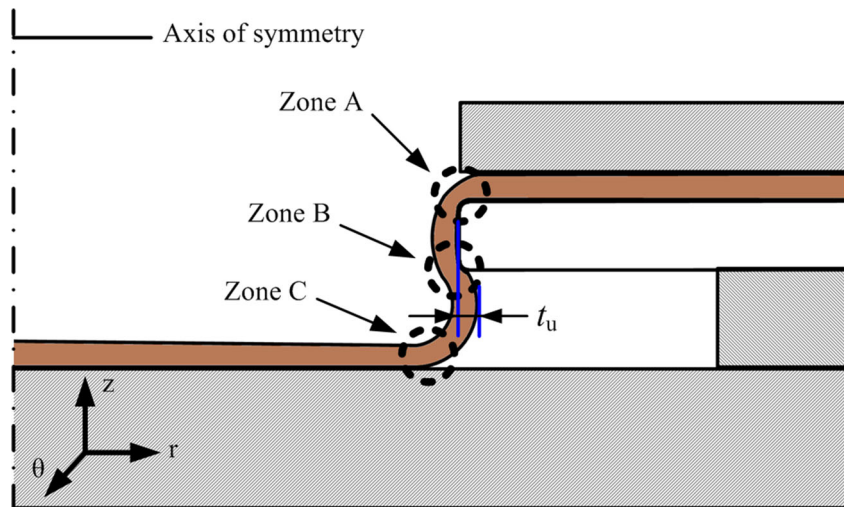


Fig. 8 Definition of three feature zones and the interlock value

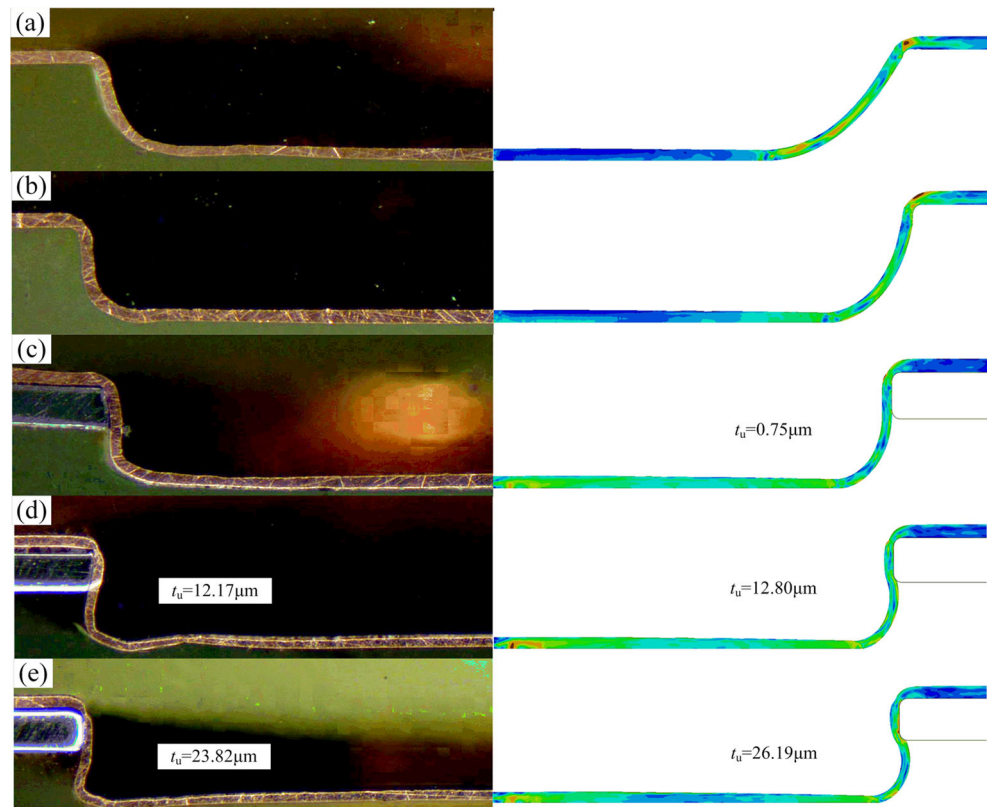


contacts with the hole wall of the joining partner II, the interlock begins to form and this stage continues until all of arranged laser pulses have been imposed.

As seen in Fig. 11a, the joining partner I is bulged into the cavity under laser shock. The plastic deformation mainly occurs along z direction in keeping with the laser incident direction. Thus, free bulging forming happens until the partner I meets the bottom plate, as shown in Fig. 11b. The length of the first stage chiefly depends on the applied laser power density, the thickness of the partner II, and the spacer height.

Figure 11c and d exhibits the metal flowing of the joining partner I in the second stage. Since the bottom plate limits the further deformation along z direction, the partner I will expand along r direction, and the region of the partner I touching the bottom plate becomes larger. In this stage, the plastic deformation focuses on the material between zone A and zone C. The material in zone A undergoes bending and stretching forming along the upper corner of the joining partner II, and gets thinner because of the constraint of blank holder. Meanwhile, zone C gradually moves along r direction with

Fig. 9 Comparison of numerical simulation and experimental measurements with various laser pulses. **a** 5; **b** 10; **c** 15; **d** 20; **e** 25



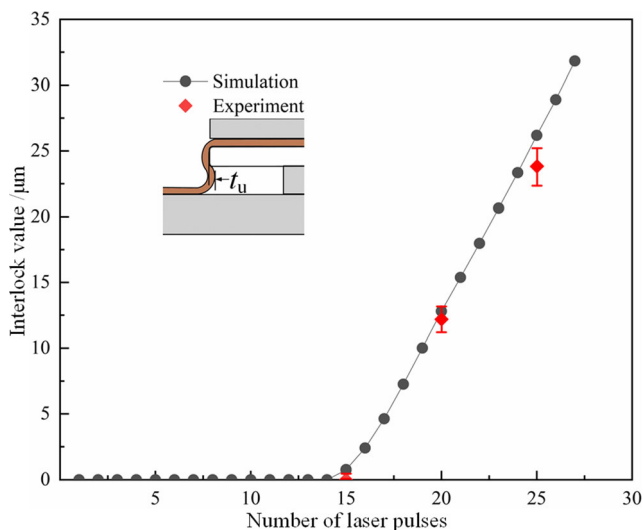


Fig. 10 Evolution of interlock value with the number of laser pulses

the increase of laser pulses. This stage lasts for several pulses until the partner I entirely contacts with the hole wall of the joining partner II, as seen in Fig. 11d.

At the end of the second stage, the two partners reach a critical state of interlock forming. As the laser pulse continuously increases, the material between zone B and zone C will expand along *r* direction, indicating that the interlock begins to form. In this stage, the material in zone B is stretched into the cavity along the lower corner of the joining partner II and zone C remains moving along *r* direction, resulting in the enlargement of interlock value. After all of the planned laser pulses have been applied, the joint with a moderate interlock value is successfully formed, as seen in Fig. 11e.

4.3 Thickness distribution of the joint

In order to examine the characteristics of thickness distribution of the clinched joint, 20 points were selected in the cross-section of the joining partner I, as seen in Fig. 12. Based on the result of the deformation stages analysis, additional points are chosen in zones A, B, and C to better capture the thickness changes.

Figure 13 presents the thickness distribution of the joining partner I of the clinched joint after 25 laser pulses. In order to better explore the thickness changes in laser shock clinching, the thinning rate η is adopted, expressed by

$$\eta = \frac{H_1 - H}{H_1} \times 100\% \tag{4}$$

where H_1 and H are the thickness of the joining partner I before and after clinching, respectively. The calculated thinning rates are also given in Fig. 13. It can be clear to see that the location of the thinnest position is in zone A, indicating that the material of the corresponding region undergoes extensive plastic deformation during laser shock clinching. Since

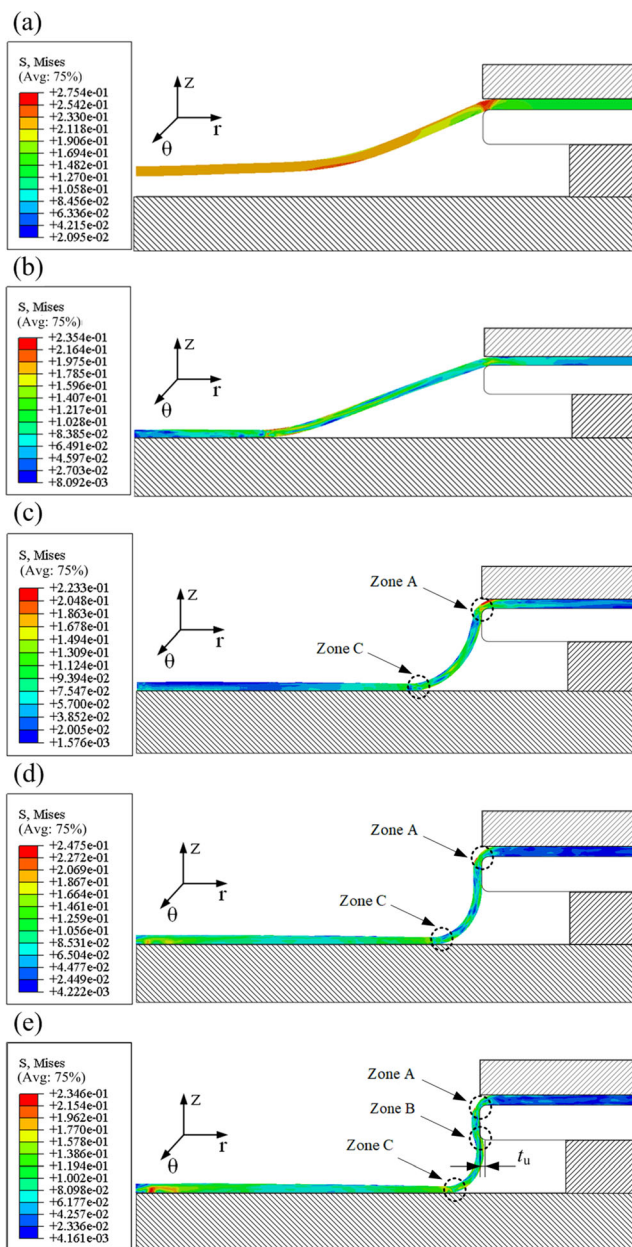
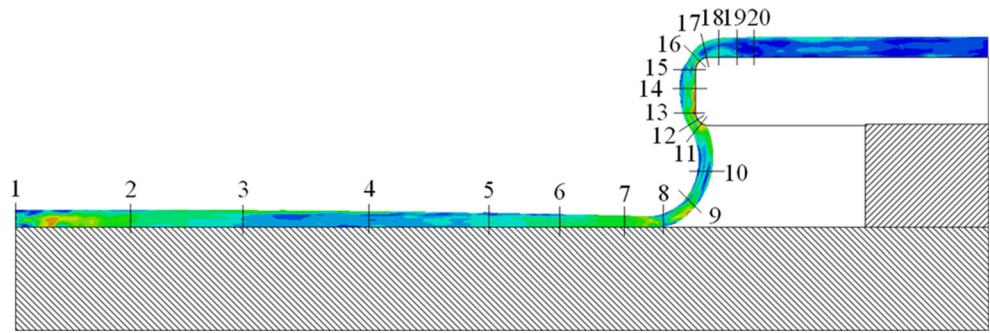


Fig. 11 Deformation stages of laser shock clinching. **a** Within the first stage; **b** the end of the first stage; **c** within the second stage; **d** the end of the second stage; **e** the end of the third stage and achievement of the joint

the material beneath the blank holder is difficult to flow into the cavity due to the confinement, the plastic deformation of the joining partner I is realized by means of thickness reduction. It is noted that the material in zone A suffers from the pressures from both laser shock wave and the small radius of the upper corner of the joining partner II. Thus, severe plastic deformation occurs in zone A, resulting in the maximum thinning rate of the whole formed joint.

As shown in Fig. 13, the thinning rate of the material in zone B is also quite large. In reference to Fig. 11d and e, as the interlock starts to form, the material in zone B is stretched into the cavity along the lower corner of the joining partner II.

Fig. 12 Illustration of measured points for thickness.



However, the material in the hole wall of the joining partner II is hard to flow due to the radial compression effect of the shock wave pressure, leading to the fact that great thinning is also inclined to appear in this region. The thinning in zone C is believed to be attributed to the axial compression effect of the shock wave pressure and the friction from the bottom plate.

4.4 Temperature rise

The temperature changes subjected to laser shock loading generally result from both the compression accompanied with the propagation of shock wave and the plastic deformation at high strain rates.

As the laser-induced shock wave compresses the metal target, it can lead to temperature rise within the target while the amplitude of shock wave pressure is large enough. The temperature rise due to shock wave compression ΔT_1 can be expressed as [30]

$$\Delta T_1 = T_0 \gamma \epsilon_V \tag{5}$$

where T_0 is the initial temperature of the material, γ is the Grüneisen constant, and ϵ_V is the volumetric strain during compression defined as

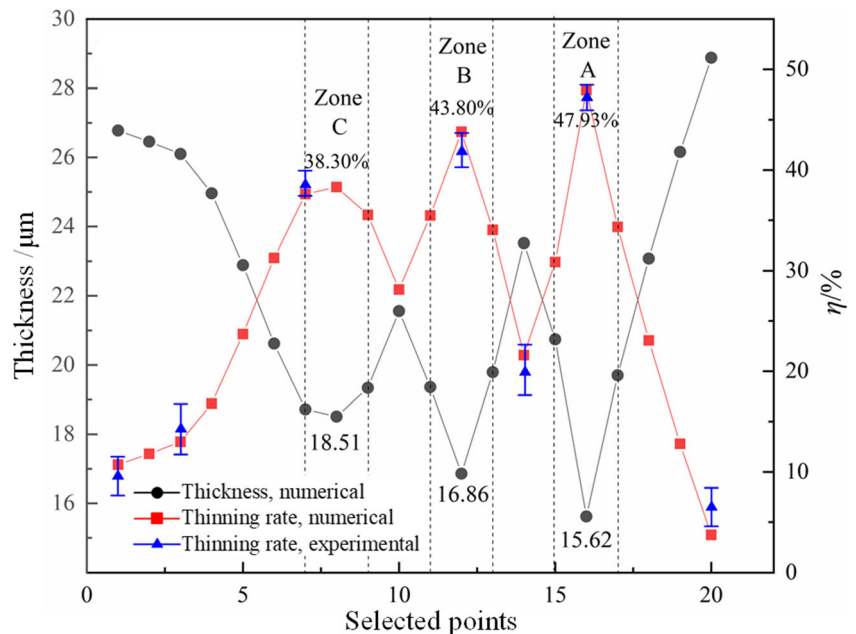
$$\epsilon_V = \frac{V_0 - V}{V_0} = 1 - \frac{V}{V_0} = 1 - \rho_0 V \tag{6}$$

where ρ_0 and V_0 is the density and specific volume at normal atmospheric pressure, respectively; V is the specific volume at shock wave pressure, given by [31]

$$V = \frac{C_0^2}{2S^2 P} \left[\sqrt{1 + \frac{4SV_0}{C_0^2} P} + \frac{2S(S-1)V_0}{C_0^2} P - 1 \right] \tag{7}$$

where C_0 is the sound velocity in the material at normal atmospheric pressure; $S \approx (\gamma + 1)/2$. For pure copper, $C_0 = 3.94 \times 10^3$ m/s, $\rho_0 = 8.93$ g/cm³, $V_0 = 0.11198$ cm³/g, $\gamma = 2.005$, and $S = 1.49$ [32]. According to Eq. (1), the amplitude of laser-induced shock wave pressure is 2.03 GPa with the laser power density of 6.76×10^{12} W/m². Thus, it is calculated that $\Delta T_1 = 0.76$ K, indicating that the effect of temperature rise due to shock wave propagation is very limited on the plastic deformation of the joining partner I.

Fig. 13 Thickness and thinning rate distribution of the joining partner I



The deformation-induced temperature rise ΔT_2 can be evaluated by the following relation [32]:

$$\Delta T_2 = \frac{\beta}{\rho_0 C_P} \int_0^\epsilon \sigma d\epsilon \tag{8}$$

where β is the Taylor coefficient and C_p is the isobaric specific heat. The Johnson–Cook model is used to describe the relationship of σ and ϵ ; refer to Eq. (2). Thus, ΔT_2 can be calculated by

$$\Delta T_2 = \left\{ 1 - \exp \left[- \frac{\beta \left(1 + C \ln \frac{\dot{\epsilon}}{\dot{\epsilon}_0} \right)}{\rho C_P (T_m - T_r)} \times \left(A \epsilon + \frac{B \epsilon^{n+1}}{n+1} \right) \right] \right\} \times (T_m - T_r) \tag{9}$$

For pure copper, $\beta = 0.9$, $A = 90$ MPa, $B = 292$ MPa, $n = 0.31$, $C = 0.025$, $m = 1.09$, $\dot{\epsilon}_0 = 1.0/s$, $T_m = 1356$ K, $T_r = 298$ K, and $C_p = 0.383$ J/(gK) [33]. The induced plastic strains under each laser pulse can be easily obtained from numerical simulation results. Thus, the temperature rise per laser pulse that arose from plastic deformation is shown in Fig. 14. It is evident that the maximum of ΔT_2 is 25.4 K, which appears in the first laser pulse. In the subsequent laser pulses, ΔT_2 is lower than 10 K, implying that there is no obvious influence of temperature increase due to high-strain-rate plastic deformation on the mechanical properties of the joining partners.

4.5 Shock wave propagation along axial direction

In laser shock processing, the shock wave propagation along axial direction, that is, the laser incident direction, is generally concerned [34]. Figure 15 presents the shock wave propagation characteristics of the first laser pulse along axial direction. In order to better explore the shock wave propagation behavior in the different positions of the joining partner I, six points are chosen along the axis of symmetry, denoted as a, b, c, d, e, and f.

As shown in Fig. 15, it can be seen that the shock wave propagation of the first laser pulse can be divided into three stages. The first stage is in the range of 0–600 ns. In this case, the stress wave exhibits a rapid increase and then attenuates to zero, which is in relation to the effect of laser-induced shock wave. The shock wave propagation of the first laser pulse in the early 50 ns is shown in Fig. 16. As the laser-induced shock wave arrives in the surface of the joining partner I, point a firstly reaches the peak value of 2.01 GPa which is close to that of the generated shock wave pressure, that is, 2.03 GPa. After that, points b–f reach the peak in order, but the peak values diminish gradually, implying that the occurrence of plastic deformation consumes part of energy. While the shock wave reaches the other surface of the joining partner I, both reflection and transmission occur, resulting in the emergence of tensile stresses. The shock wave then attenuates in a vibration mode and finally turns into zero.

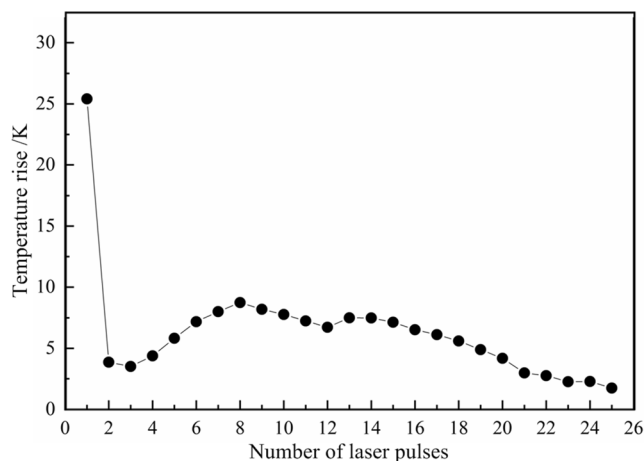


Fig. 14 Temperature rise per laser pulse due to plastic deformation

The second stage is within 600–2900 ns with a manifest feature that the stress values of six points equal to zero, as seen in Fig. 15. It is noted that the deformation of the joining partner I in this stage involves with the free bulging forming; refer to Fig. 11a. Though the stresses are zero, the plastic deformation continues due to the inertial effect [35]. At about 2900 ns, the pure copper foil contacts with the bottom plate.

The third stage lasts from 2900 to 5000 ns, as seen in Fig. 15. At the end of the second stage, the pure copper foil touches the bottom plate at high velocity, and then the crash introduces a new stress wave which propagates into the pure copper foil again. The new stress wave spreads from point f to a, and while it arrives in the other foil surface, both reflection and transmission also occur. Then the values of the generated stress wave decline gradually accompanied by further plastic deformation.

Figure 17 presents the shock wave propagation characteristics of the second laser pulse along axial direction. Due to the fact that the pure copper foil has contacted with the bottom

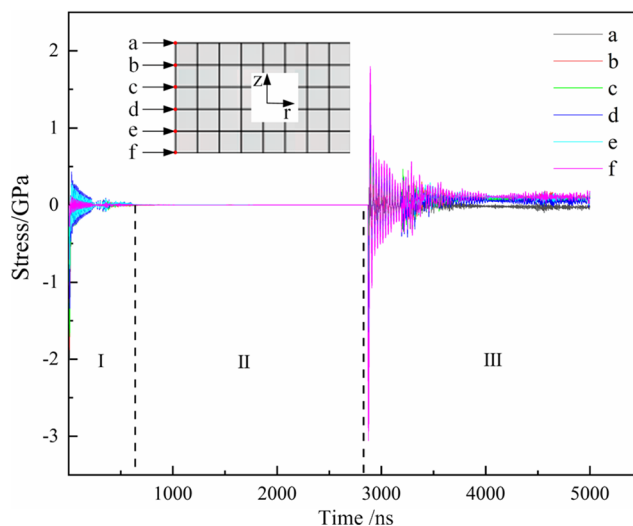


Fig. 15 Shock wave propagation characteristics of the first laser pulse along axial direction

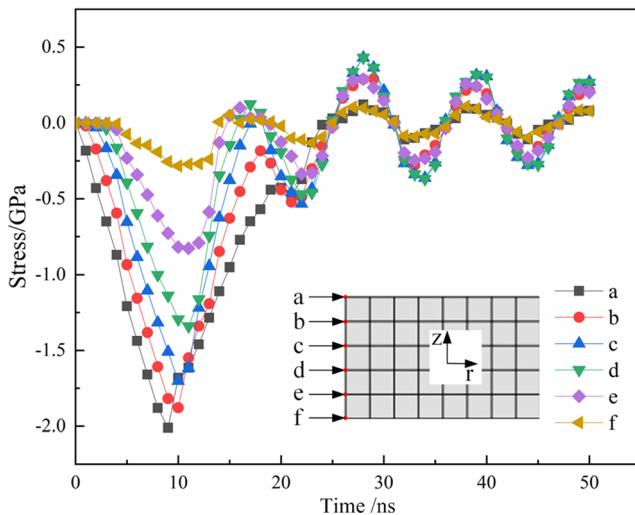


Fig. 16 Shock wave propagation of the first laser pulse in the early 50 ns

plate after the first laser pulse, there are two types of stress wave propagation within the second laser shock. One is the shock wave induced by the second laser pulse which propagates from point a to f, and the other is the response of the bottom plate to the induced shock wave followed by a reverse stress wave which propagates from point f to a. The two types of stress wave mutually interfere within the pure copper foil accompanied with reflection and transmission, and gradually turn into zero. It is noted that the shock wave propagation of the subsequent laser pulses along axial direction exhibits the same trend to that of the second pulse.

4.6 Effect of laser power density

It is well known that laser power density is one of essential parameters to determine the formation and performance of the part in laser shock processing. Thus,

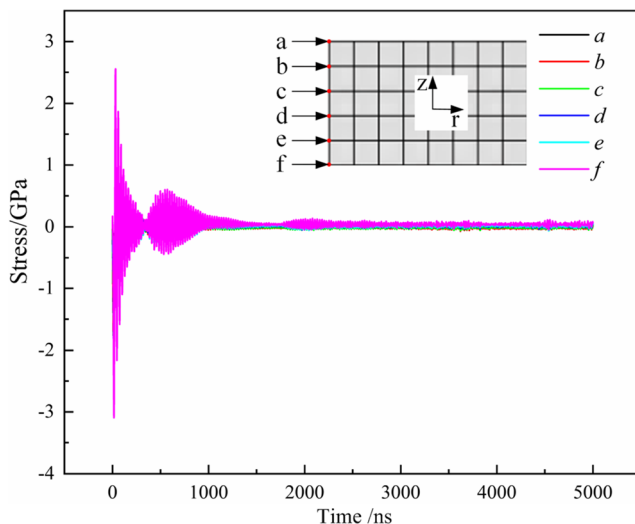


Fig. 17 Shock wave propagation characteristics of the second laser pulse along axial direction

the effect of laser power density on the interlock value and thickness distribution is concerned based on the numerical simulation. A range of 4.80×10^{12} to 1.09×10^{13} W/m² is adopted. According to the previous experimental researches, the obtained interlock value can equal to or even exceed the original thickness of the joining partner I without fracture [18, 19, 24]. As a consequence, the calculation of the aforementioned laser power densities lasts until the interlock value reaches or slightly surpasses 30 μm, relying on the effect of the last applied pulse.

Figure 18 presents the evolution of interlock value under various laser power densities. It can be apparently seen that the threshold of laser pulse beginning to form interlock decreases with the enhancement of laser power density. While the interlock starts to develop, the increment of per laser pulse becomes larger as the laser power density is strengthened, implying that fewer pulses are needed to accomplish the same interlock value. According to Eq. (1), obviously the amplitude of the shock wave pressure can be amplified while a higher laser power density is applied, leading to the increase of the plastic deformation degree of the joining partner I and thus the earlier formation of the interlock.

Figure 19 shows the thickness distribution under various laser power densities while the interlock value is about 30 μm. The measured positions are in accordance with those in Fig. 12. It can be seen that the thickness distribution presents a similar trend among the given laser power densities. The thinnest region locates in zone A, implying that crack may appear in this region if too high laser power density is applied.

The relationship of the maximum thinning rate and laser power density is shown in Fig. 20. It can be seen that while the laser power density is in the range of 4.80×10^{12} to 8.72×10^{12} W/m², the maximum thinning rate is between 46.8 and

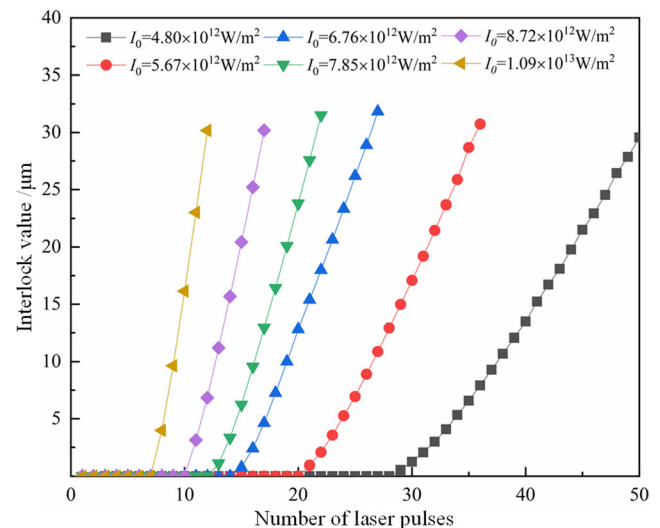


Fig. 18 Evolution of interlock value under various laser power densities

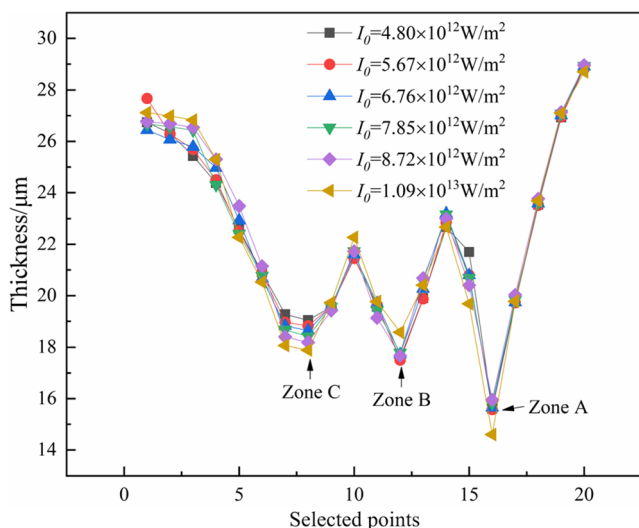


Fig. 19 Thickness distribution under various laser power densities

48.1%. However, when the laser power density is strengthened to $1.09 \times 10^{13} \text{ W/m}^2$, the maximum thinning rate rises to 51.3%. Obviously, the excessive reduction in thickness has an adverse effect on the performance of the clinched joint and even leads to the occurrence of fracture. Thus, the reasonable arrangement of laser power density should be considered in order to obtain a clinched joint with a moderate interlock value and high joining efficiency.

5 Conclusions

In the present paper, the mechanical joining behavior of pure copper foil and pre-pierced stainless steel sheet in laser shock clinching was investigated through numerical simulation approach. The characteristics of the deformation stages, thickness change, temperature increase, shock wave propagation as

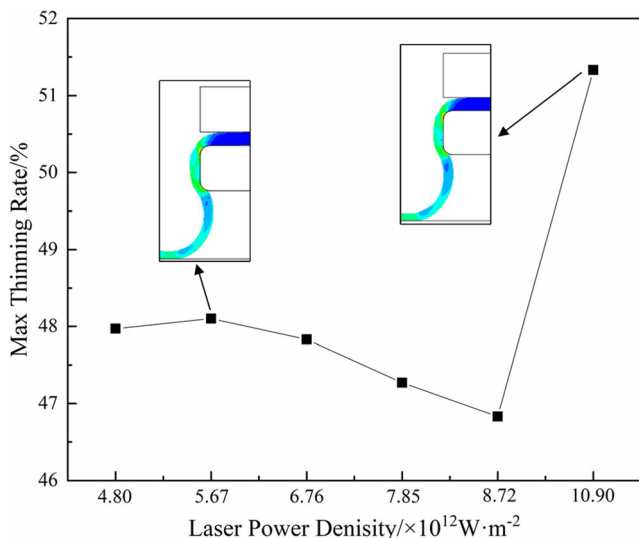


Fig. 20 The maximum thinning rate under various laser power densities

well as the effect of laser power density were examined. The following conclusions are drawn from this research:

1. Laser shock clinching process can be divided into three deformation stages, that is, free bulging forming, radial expansion, and formation of interlock. Both experimental and numerical results prove that the formation of clinched joints relies on the plastic deformation of the joining partner I.
2. The thinnest region of the joint locates at the material of the joining partner I in contact with the upper corner of the joining partner II, which is related to the confinement of blank holder and the pressures from both laser shock wave and the small radius of the upper corner of the partner II.
3. The temperature increases that arose from the compression by shock wave and plastic deformation at high strain rates are quite small. Thus, there is no obvious influence of temperature increase on the mechanical properties of the joining partners.
4. The shock wave propagation along axial direction of the first laser pulse can be divided into three stages, while there are two types of stress wave propagation for the second and subsequent laser shock. The attenuation, reflection, transmission, and interaction of stress waves exist within the metal foil accompanied with plastic deformation.
5. Laser power density plays a significant role in the threshold of laser pulse beginning to form interlock and the necessary number of pulses to accomplish the expected interlock value. However, there are no obvious changes in the thickness distribution and the thinnest region of joints under the given laser power densities.

In addition, the present research focuses on the numerical simulation investigation in the mechanical joining behavior of two metallic dissimilar materials. In the further work, the problem in the development of absorbent coating materials with high efficiency and easy operation will be studied. Moreover, the effect of other laser parameters and properties of joining partners on the clinching defects, joint performance as well as failure modes of the clinched joint will be discussed.

Acknowledgments This work is supported by the National Natural Science Foundation of China (No. 51205232), Natural Science Foundation of Shandong Province (No. ZR2017BEE006), and the Fundamental Research Funds of Shandong University (2018JC042).

Compliance with ethical standards

Conflict of Interest The authors declare that they have no conflict of interest.

References

1. Eshtayeh MM, Hrairi M, Mohiuddin AKM (2016) Clinching process for joining dissimilar materials: state of the art. *Int J Adv Manuf Technol* 82:179–195
2. Chua SF, Chen HC, Bi GJ (2019) Influence of pulse energy density in micro laser weld of crack sensitive Al alloy sheets. *J Manuf Process* 38:1–8
3. Shi WQ, Wang WH, Huang YL (2016) Laser micro-welding of Cu–Al dissimilar metals. *Int J Adv Manuf Technol* 85:185–189
4. Zimmer K, Ehrhardt M, Lorenz P, Stephan T, Ebert R, Braun A (2013) Joining of molybdenum thin films with copper printed circuit board by laser micro-riveting. *Opt Laser Technol* 49:320–324
5. Lerra F, Ascari A, Fortunato A (2019) The influence of laser pulse shape and separation distance on dissimilar welding of Al and Cu films. *J Manuf Process* 45:331–339
6. Shi WQ, Huang J, Xie YP, Li YQ, An FJ (2017) Laser micro-welding technology for Cu–Al dissimilar metals and mechanisms of weld defect formation. *Int J Adv Manuf Technol* 93:4197–4201
7. Chen YH, Mao YQ, Lu WW, He P (2017) Investigation of welding crack in micro laser welded NiTiNb shape memory alloy and Ti6Al4V alloy dissimilar metals joints. *Opt Laser Technol* 91:197–202
8. Remington TP, Remington BA, Hahn EN, Meyers MA (2017) Deformation and failure in extreme regimes by high-energy pulsed lasers: a review. *Mater Sci Eng A* 688:429–458
9. Zhang Y, Babu SS, Prothe C, Blakely M, Kwasegroch J, LaHa M, Daehn GS (2011) Application of high velocity impact welding at varied different length scales. *J Mater Process Technol* 211:944–952
10. Wang HM, Vivek A, Wang YL, Taber G, Daehn GS (2016) Laser impact welding application in joining aluminum to titanium. *J Laser Appl* 28:032002
11. Wang X, Gu CX, Zheng YY, Shen ZB, Liu HX (2014) Laser shock welding of aluminum/aluminum and aluminum/copper. *Mater Des* 56:26–30
12. Wang HM, Taber G, Liu DJ, Hansen S, Chowdhury E, Terry S, Lippold JC, Daehn GS (2015) Laser impact welding: design of apparatus and parametric optimization. *J Manuf Process* 19:118–124
13. Wang X, Huang T, Luo YP, Liu HX (2017) Laser indirect shock welding of fine wire to metal sheet. *Materials* 10:1070
14. Wang HM, Wang YL (2017) Laser-driven flyer application in thin film dissimilar materials welding and spalling. *Opt Lasers Eng* 97:1–8
15. Mori K, Abe Y (2018) A review on mechanical joining of aluminum and high strength steel sheets by plastic deformation. *Int J Light Mater Manuf* 1:1–11
16. Groche P, Wohletz S, Brenneis M, Pabst C, Resch F (2014) Joining by forming—a review on joint mechanisms, applications and future trends. *J Mater Process Technol* 214:1972–1994
17. Ji Z, Liu R, Wang DG, Zhang MH, Su QC (2008) A micro clinching method and its device for joining ultrathin sheets with pulsed laser. Chinese Patent ZL200810014018.1
18. Veenaas S, Wielage H, Vollertsen F (2014) Joining by laser shock forming: realization and acting pressures. *Prod Eng Res Dev* 8:283–290
19. Veenaas S, Vollertsen F (2014) High speed joining process by laser shock forming for the micro range. 6th International Conference on High Speed Forming, Daejeon, Korea, pp 97–105
20. Veenaas S, Vollertsen F (2015) Forming behavior during joining by laser induced shock waves. *Key Eng Mater* 651–653:1451–1456
21. Wang X, Li C, Ma YJ, Shen ZB, Sun XQ, Sha CF, Gao S, Li LY, Liu HX (2016) An experimental study on micro clinching of metal foils with cutting by laser shock forming. *Materials* 9:571
22. Wang X, Li XD, Li C, Shen ZB, Ma YJ, Liu HX (2018) Laser shock micro clinching of Al/Cu. *J Mater Process Technol* 258:200–210
23. Wang XY, Ji Z, Wang JF, You SX, Zheng C, Liu R (2018) An experimental and numerical study on laser shock clinching for joining copper foil and perforated stainless steel sheet. *J Mater Process Technol* 258:155–164
24. Wang XY, Ji Z, Liu R, Zheng C (2018) Making interlock by laser shock forming. *Opt Laser Technol* 107:331–336
25. Li XD, Wang X, Shen ZB, Ma YJ, Liu HX (2019) An experimental study on micro-shear clinching of metal foils by laser shock. *Materials* 12:1422
26. You SX, Wang XY, Ji Z, Zheng C, Zhang GF, Liu R (2019) Making line undercut structure by incremental laser shock forming. *Int J Precis Eng Manuf* 20:1289–1296
27. Fabbro R, Fournier J, Ballard P, Devaux D, Virmont J (1990) Physical study of laser-produced plasma in confined geometry. *J Appl Phys* 68:775–784
28. Zheng C, Pan CD, Tian ZR, Zhao XH, Zhao GQ, Ji Z, Song LB (2020) Laser shock induced incremental forming of pure copper foil and its deformation behavior. *Opt Laser Technol* 121:105785
29. Johnson GR, Cook WH (1983) A constitutive model and data for metals subjected to large strains, high strain rates and high temperatures, 7th International Symposium on Ballistics. Hague, Netherlands, pp 541–547
30. Fan SQ (2007) Study on the dynamic responses and failure of cylindrical shell subjected to typical explosive loadings. Dissertation, University of Science & Technology of China
31. Ye YX, Xuan T, Lian ZC, Feng YY, Hua XJ (2015) Investigation of the crater-like microdefects induced by laser shock processing with aluminum foil as absorbent layer. *Appl Surf Sci* 339:75–84
32. Meyers MA (1994) Dynamic behavior of materials. John Wiley & Sons, Inc., Hoboken
33. Ryazanov AI, Pavlov SA, Kiritani M (2003) Effective temperature rise during propagation of shock wave and high-speed deformation in metals. *Mater Sci Eng A* 350:245–250
34. Fan Y, Wang Y, Vukelic S, Yao YL (2005) Wave-solid interactions in laser-shock-induced deformation processes. *J Appl Phys* 98:104904
35. Rusinek A, Zaera R, Klepaczko JR, Cheriguene R (2005) Analysis of inertia and scale effects on dynamic neck formation during tension of sheet steel. *Acta Mater* 53:5387–5400

Publisher's note Springer Nature remains neutral with regard to jurisdictional claims in published maps and institutional affiliations.